POLITECNICO DI TORINO

Dipartimento di Energia

Corso di Laurea Magistrale

Innovazione in sistemi per la produzione di energia

Tesi di Laurea Magistrale

Simulation of performance and degradation of novel electrocatalyst

Relatori

Stefania Specchia

Bradley Easton

Candidato

Paolo Piovano

Ottobre 2018

DEDICATION

I dedicate this project to my girlfriend and my family. Without them I wouldn't have found the motivation and the energies to conduct this project and carry on with the whole degree as well. They represent the driving force of my life.

Index

1. Introduction

1.1 Technology description

Proton exchange membrane fuel cell (PEMFC) is a technology that has gained more and more importance in the energy sector during last decades: it's suitable for automotive applications, distributed energy production systems from small size for residential consumers to big size for industrial users and for portable electronic devices. It is considered a promising solution in future energy production infrastructure because of several strong points. It shows nominal efficiency higher than 50% (that further increases at partial loading) and has a high-power density; it is easy to install, requires little maintenance because of the lack of moving part, has very short starting time and a low noisy level. Moreover, it can be considered a partial solution to current environmental issues linked to carbon dioxide emissions as the high efficiency involves a low CO_2 emission rate per produced energy unit; in addition, other pollutants usually emitted by traditional combustion-based power plants as carbon monoxide, silicon and nitrogen oxides are totally avoided. For all these reasons, a lot of efforts are being made in research to improve performance and decrease prices.

Fuel cell is an electrochemical device that transforms the chemical energy stored in a fuel (for example hydrogen for PEMFC) directly into electrical energy, with high efficiency and without passing through a thermal cycle. The by-products are water that comes from the hydrogen oxidation and heat released because of unavoidable irreversibilities, such as mass transport and ohmic losses.

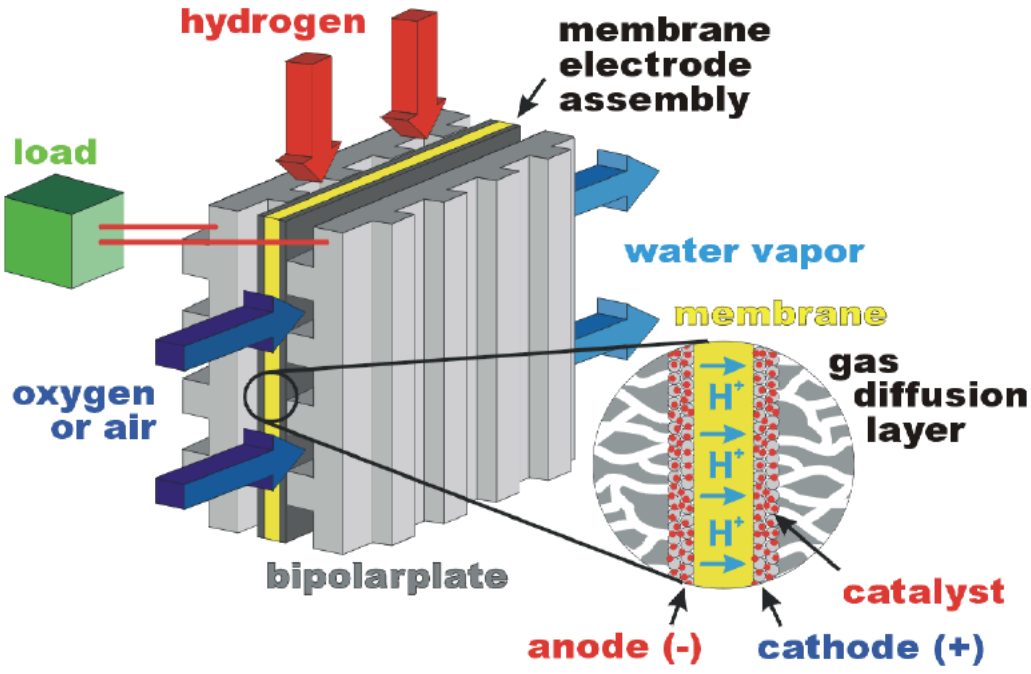

Fig. 1-1 *Components and mass streams of a PEM fuel cell*

As shown in figure 1-1, the machine is formed by a multi-layered structure: its core component, the membrane-electrode assembly (MEA), has a proton conducting membrane layer sandwiched between two electrodes: anode and cathode; each electrode consists of a very thin catalyst layer (CL) deposited on a gas diffusion layer (GDL). During the operation, hydrogen and oxygen are transported through the pore regions of the anode and cathode GDLs respectively to the reaction sites within the CLs: there, hydrogen is oxidised into H^+ ion and electron while oxygen is reduced

producing water. The following represents hydrogen oxidation reaction (HOR), oxygen reduction reaction (ORR) and total hydrogen combustion reaction simply resulting from the sum of the previous:

HOR	$2H_2 \rightarrow 4H^+ + 4e^-$	(1)
ORR	$O_2 + 4H^+ + 4e^- \rightarrow 2\ H_2O$	(2)
Total	$2H_2 + O_2 \rightarrow 2\ H_2O$	(3)

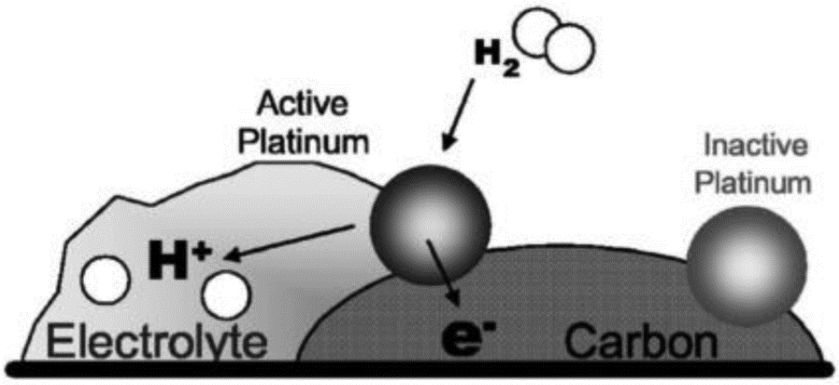

Fig. 1-2 *Hydrogen oxidation on an active Pt site*

Figure 1-2 shows a reaction site, also known as three-phase-boundary because formed by the interconnection of three different materials: the catalyst (often electrochemically active Pt) permits the reaction to take place; the carbon support represents a preferential way for the electrons; the ionomer binder (usually Nafion) is a pathway for the H^+ ions that leaves the reaction point within the anodic CL towards the membrane. For a proper exploitation of the whole precious Pt used in the CL it's fundamental an homogeneous interconnection among each Pt particle and both ionomer and carbon; this is achieved with a highly dispersed microstructure with a high surface area. In this way, reactants particles can percolate deeply within the CL and be in contact with a large number of active reaction sites.

1.2 Project purpose

Present work is aimed to better understand the future role of PEMFC as distributed power production systems: the performance of a traditional commercial Nafion based electrocatalyst will be compared to a novel one under study in the host university from an energetic point of view, imagining to use them in a PEMFC stack for a residential purpose.
The conventional catalyst layer is composed of platinum supported on carbon (Pt/C) with Nafion ionomer as a proton conductor; on the other hand, the innovative electrocatalyst under research is a sulfonated-silica ceramic carbon electrode (SS-CCE) that employs metal oxides as supporting materials; SS-CCE has been already tested long in literature, proving to be a promising candidate for application in PEMFCs [1]. The performance in terms of maximum power density are comparable to the Nafion based electrodes, but its most remarkable feature lays in the degradation response: as discussed later, the SS-CCE manages to stabilize in a better way the Pt nanoparticles, slowing its rate of agglomeration and maintaining good performance for longer.
In the first part, the static behaviour of a single cell at the beginning of life is computationally modeled in Matlab environment in order to predict performance and the outcome is tested comparing the actual results measured in laboratory. Later, moving to the dynamic operation high attention is addressed to the time-depending degradation processes that worsen in a non-negligible

way the efficiency of the whole stack during the useful lifespan. The model previously developed for the static performance is then upgraded to predict the behaviour under degradation. From an electrochemical point of view, Pt nanoparticles contained in the electrode decrease their activity following Ostwald ripening, agglomeration and dissolution into the ionomer phase. These three phenomena are token into consideration to model and predict the performance decay.

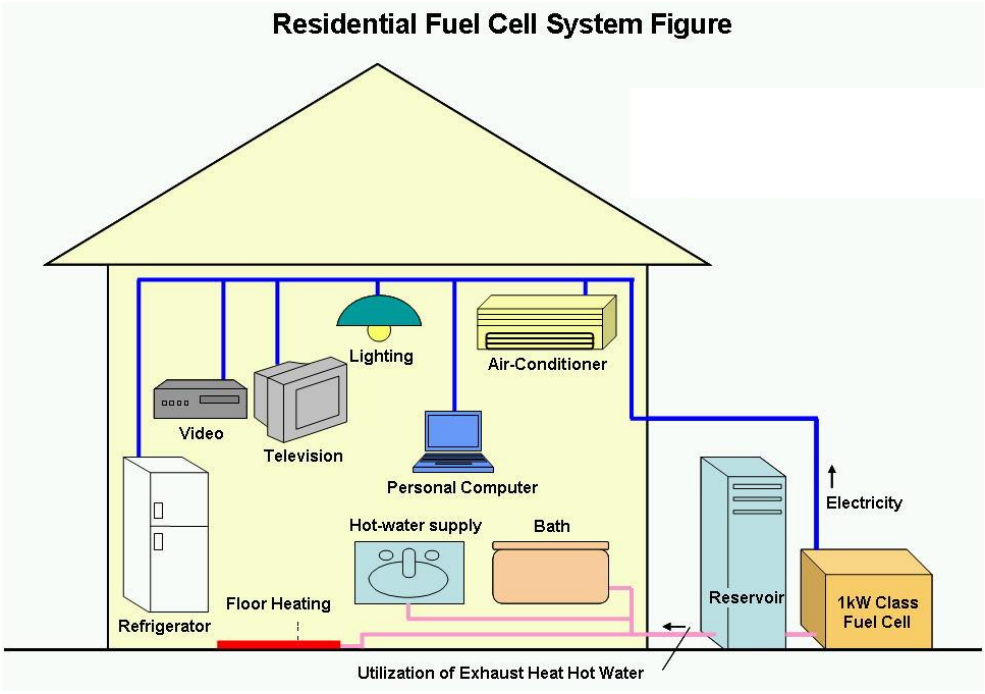

Fig. 1-3 *Schematic of a µCHP system based on a PEM fuel cell*

A real case study of a micro-cogeneration heat and power (µCHP) system for a residential purpose is analysed from an energetic point of view. Distributed power production unit is one of the most interesting application of PEMFC whereas it permits to produce locally electrical power having access to a natural gas and therefore to partially detach from the electrical grid; nowadays the natural gas grid is widespread in most part of Europe and North America. The future target is to consider the final user not only as a passive consumer but an active producer that acts a double-direction energy exchange with the electrical grid (the so-called prosumer) in order to achieve a higher degree of independency in energy supply. The heat released from the stack is considered an useful product as it can heat water for domestic purpose and air conditioning. Other advantages of a µCHP system are high natural gas-to-power efficiency, easy control, null maintenance and high reliability, together with the competitivity in the energy market. Also the high environmental sustainability as a result of the high efficiency is a big advantage. For all these reasons, µCHP installations in residential housing were incentivized from government in past years all over Europe (Callux, Enefield and PACE projects) and Japan (ENE-FARM project), permitting the installation of thousands of units. In this work, real statistical data of Canadian households are used to analyse the energetic balance. In figure 1-3 is shown how a fuel cell can support the load of all domestic devices supplying both electric and thermal energy.
In fig 1-4, an energetic balance is made comparing the traditional domestic energy production with a µCHP system in a qualitative way. Starting from the same useful energy output (1 thermal MWh plus 1 electric MWh), using estimations of average typical values of efficiency it's possible to evaluate the CO_2 emission rate; for the fuel cell technology it is decreased of 30%, meaning that it

represents an energy production solution more sustainable with respect to the old combustion-based systems.

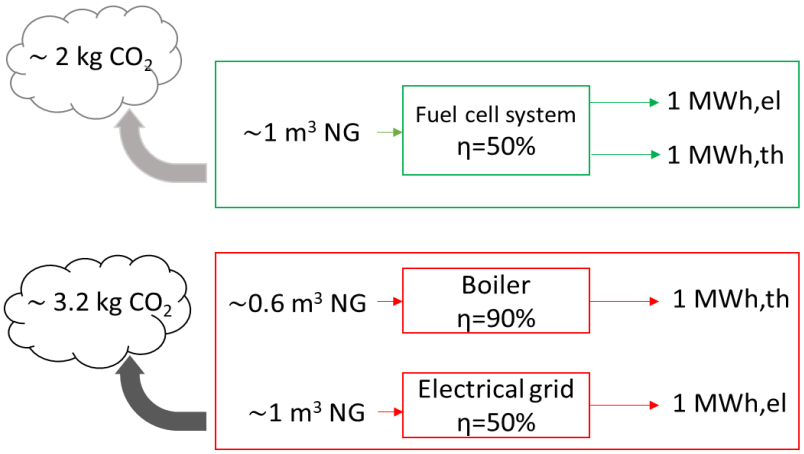

Fig. 1-4 *Comparison in carbon emission rate of traditional vs fuel cell technology*

2. EXPERIMENTAL

The preparation of the traditional Nafion-based electrode follows this procedure. A Premetek Pt-C catalyst is employed; the amount of Pt-C used was chosen to obtain a final loading on both anode and cathode of 0.18 mg/cm^2. The solution of water, Nafion, isopropanol and Pt was stirred for 2 hours, sonicated for 1 hour and then stirred again for one night.

Electrocatalyst specifications	Catalyst	Premetek
	Pt-C ratio	20%
Solution composition	Pt-C [mg]	48
	Water content [mg]	4
	Nafion content [ml]	0.3
	IPA content [mg]	1.25
	GDL	29 BC
Final electrode characteristics	Pt loading [mg/cm^2]	0.18
	Nafion loading [mg/cm^2]	0.38

Table 1-1 Nafion-based electrode characterization

The electrode was prepared by spray depositing the Pt-C solution with an air gun directly onto a carbon paper gas diffusion layer; 29 BC was chosen as GDL because of its good performance in removing water. The Nafion 212 membrane was dried at 60 °C and then sandwiched between two 5 cm^2 wide electrodes. The membrane electrode assembly (MEA) was hot pressed at 100 °C for 3 minutes under a pressure of 40 kg/cm^2 in order to have a good contact between electrode and the membrane, preventing at the same time the destruction of the surface morphology. Afterwards, at both sides of the MEA was added a sealing gasket and the whole set was put together in the cell. Fig. 2-1b shows the total sandwich of electrodes (black), Nafion membrane (transparent) and the sealing gasket (white). The plates have snake-shaped reactant channels that ensures an homogeneous distribution of the species over the whole electrode surface (fig 2-1a). MEAs were tested in a 5 cm^2 fuel cell on a commercial fuel cell test station (Fuel Cell Technologies) controlled using Labview software.

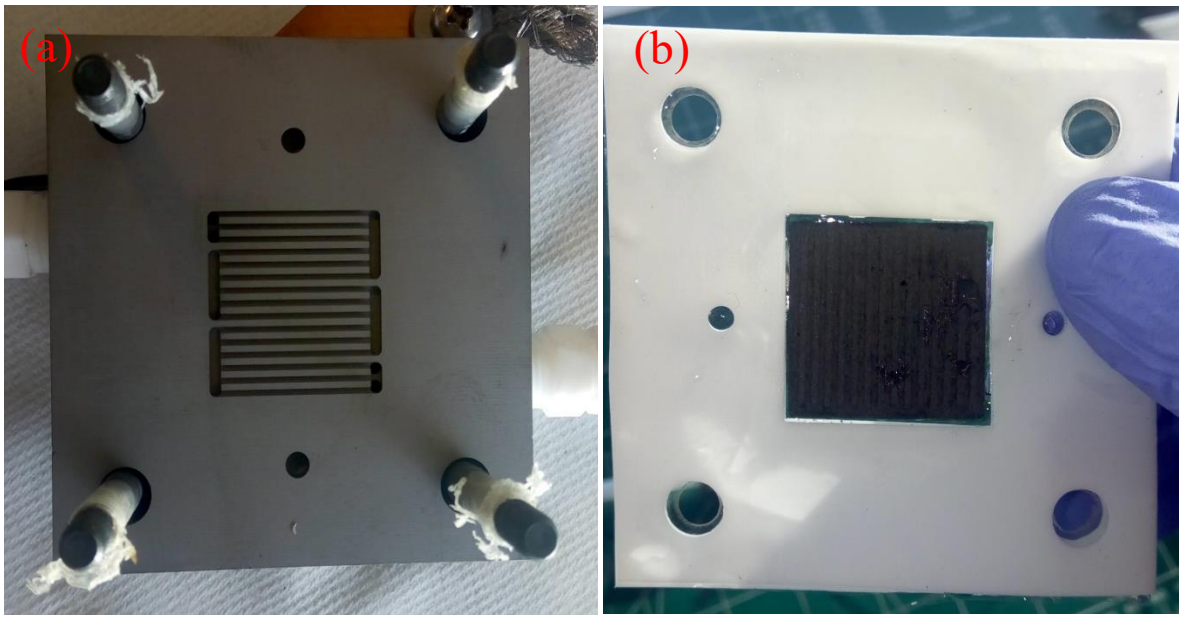

Fig. 2-1 *(a) plate used to sandwich the MEA. The reactant channel is snake-shaped and (b) MEA with sealing gasket*

3. MODEL DESCRIPTION

3.1 Static performance model

In the first part of the project the target is to model the performance of a single PEM fuel cell: that will be useful when simulating the behaviour of the real stack in a residential application.
Peppley et al. [2] developed a simplistic but reliable deterministic model able to compute the polarization curve starting from some characteristic features and operating conditions; since the model is believed to be trustworthy only at low-medium current density levels, an additional source was incorporated to explain the behaviour at high current density [3]. The simulation outcome was validated against the actual polarization curve measured in laboratory.
The model is called general steady state electrochemical model (GSSEM) and can be implemented in Matlab environment starting from dimensional characteristic, cell area, membrane thickness, electrode electrochemical surface area and operating conditions such as the anodic and cathodic pressure, relative humidity, current density and cell temperature; the model should be able to describe performances of a cell built with a commercial electrode as well as a cell using a novel one.
The GSSEM is a bit old and simplistic but still sufficiently trustworthy as it derives from a deterministic description of PEMFC supplied by some statistical techniques. The output is the polarization curve, that describes the voltage response at different current density levels. The typical shape of a PEMFC polarization curve is shown in fig. 3-1: it's possible to distinguish three different regions along the horizontal axis in which distinct loss processes are predominant. The first steep decrease is due to the charge transfer loss, caused by the energetic barrier that must be overcome to start the electrochemical reaction (regarding both electrodes), after breaking the equilibrium. The second loss is considered linear and it's due to the charge conduction (H^+ ions) in a conductive material (Nafion membrane). Finally, at high current density levels the main source of voltage loss is due to mass transport phenomena: the reactant flows are so high that the reaction is limited by mass transport resistance within the GDLs.

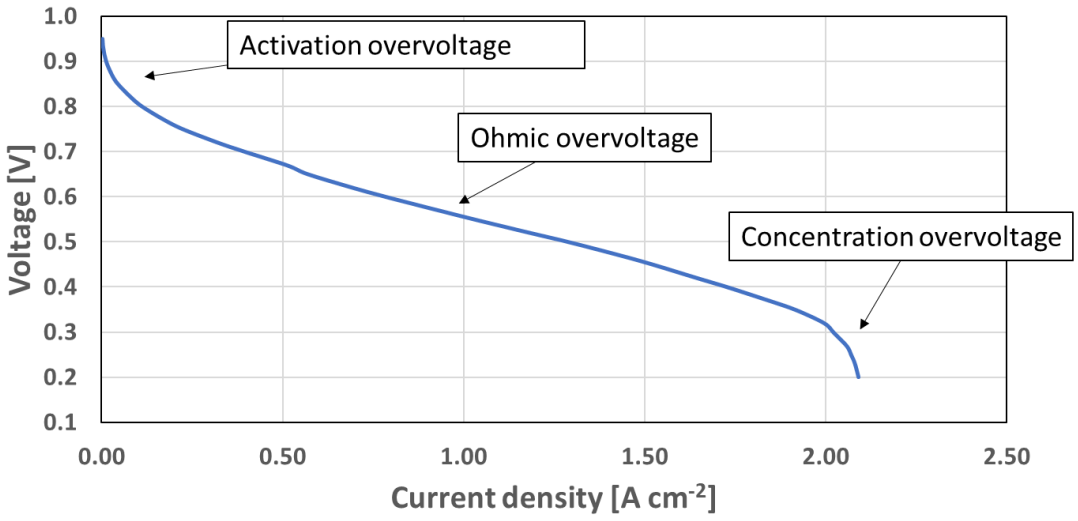

Fig. 3-1 *Typical fuel cell polarization curve*

This description of the voltage response makes analytically suitable an expression like (1), in which a certain amount of potential is subtracted for each loss mechanism starting from the ideal open circuit voltage:

$$V_{cell} = OCV + \eta_{act,an}(i) + \eta_{act,cath}(i) + \eta_{ohm}(i) + \eta_{\mathrm{conc}}(i) \quad [V] \qquad (1)$$

where OCV is the open circuit voltage, $\eta_{\mathrm{act,an}}$ and $\eta_{\mathrm{act,cath}}$ are anode and cathode activation overvoltage respectively, η_{ohm} is the ohmic overvoltage and η_{conc} is the concentration overvoltage. All the overvoltage values in eq. (1) are negative and depend on the current density. Each term will be separately discussed and modelled in the following treatise.
Nernst equation provides the ideal open circuit voltage (at null current) for the hydrogen oxidation reaction and can be written as follows:

$$OCV = E^0(T) + \frac{RT}{nF}\ln(p_{H_2}(p_{O_2}^{0.5})) \quad [V] \qquad (2)$$

in which E^0 is the reference potential and is a thermodynamic value depending only on the temperature; as the temperature T will be fixed during all the experiments at 80°C , the reference potential shows a calculated value of 1,182 V. The terms p_{H_2} and p_{O_2} represent respectively the partial pressure of hydrogen at the anodic catalyst/gas interface and the partial pressure of oxygen at the cathodic catalyst/gas interface. R is the ideal gas constant, F is the Faraday constant and n is the number of electron exchanged per reactant mole in a single reaction (n=2 for hydrogen).
The activation overvoltage is obtained with a Tafel approximation and it's attributed predominantly to the cathodic reaction since the oxygen reduction reaction (ORR) has a slower kinetic with respect to the anode oxidation. Eq. (3) shows only the cathodic correlation but for the anode is totally analogue.

$$\eta_{act,\,cath} = \frac{2.3\,RT}{\alpha nF} ln\left(\frac{i_0}{i}\right) \quad [V] \qquad (3)$$

in which i_0 is the exchange current density and α is the transfer coefficient. The exchange current density is an estimation of the speed of the reaction: the higher the exchange current density, the faster the reaction is to be activated; it is evaluated with an empirical correlation:

$$i_{0,cath} = nFAk\left[exp\left(\frac{-\Delta G}{RT}\right)(c_{O_2})^{(1-\alpha)}(c_{H^+})^{(1-\alpha)}(c_{H_2O})^{\alpha}\right] \quad [A] \qquad (4)$$

i_0 depends on electrochemical values, all tabulated in literature, such as the rate constant (k) and variation of Gibbs free energy of chemisorption (ΔG). It's important to notice its dependence on the concentration at the interface between membrane and CL of O_2, H_2O and H^+ ions. The H^+ ion concentration is easily obtainable from the electroneutrality law which requires that it is equal to the sulfonic acid ion concentration in the membrane, that is imposed by the Nafion structure and fixed during the experiments. On the other hand, to compute the reactant and product concentration starting from the bulk flow pressures, a mass transport analysis is required.
The spatial domain covered by the flows is split in two regions: firstly, the reactants that leave the channel must diffuse within the porous electrode and successively they must percolate through the water film that may cover the catalyst layer. The diffusion model through the gas diffusion layer gives an estimation of the pressure drop that the reactant flow experiences; it's calculated integrating a Stefan-Maxwell diffusion equation between the flow channel and the catalyst surface, assuming the flow direction to be one-dimensional and normal to the surface of the electrode.

$$\frac{dx_{O_2}}{dz} = \frac{RT}{P\,D_{H_2O,O_2}^{eff}}(x_{H_2O} * N_{O_2}) \qquad (5)$$

In equation (5), P represents the total channel pressure (Pa), D_{H_2O,O_2}^{eff} is the effective binary diffusivity for the H_2O-O_2 pair in the porous medium and N_{O_2} is the oxygen molar flow.

Successively, it is necessary to analyze the transport of dissolved gas through the water film; this water film isn't believed to create a significant barrier to gas transportation and we can assume that all the dissolved reactant gas is in equilibrium with the bulk gas. Then a Henry law is applied using available solubility data (eq. 6).

$$c_{O_2} = \frac{p_{O_2,\,interface}}{5.08 * 10^6 exp(\frac{-498}{T})} \tag{6}$$

In both equation (5) and (6) many values are considered constant and can be found in literature. The ohmic overvoltage η_{ohm} represents a measure of the losses associated to the proton conductivity of the solid polymer electrolyte and electronic internal resistances (carbon support and bipolar plates) and it's calculated with a typical Ohm equation:

$$\eta_{ohm} = -i * r_M \frac{l}{A} \qquad [V] \tag{7}$$

The electronic resistance can be considered negligible with respect to the ionic membrane resistance (r_M) since there are many orders of magnitude difference between those. Eq. (7) contains both dimensional features (cell area and membrane thickness) and physical characteristic. The Nafion membrane specific resistivity r_M is worked out using a semi-empirical correlation, as shown in eq. (8):

$$r_M = \frac{181.6 * \left[1 + 0.03 * \left(\frac{i}{A}\right) + 0.062 \left(\frac{T}{303}\right)^2 \left(\frac{i}{A}\right)^{2.5}\right]}{\left[\lambda - 0.634 - 3\left(\frac{i}{A}\right)\right] exp[3.25\left(\frac{T-303}{T}\right)]} \qquad [\Omega\, cm] \tag{8}$$

The membrane specific resistivity depends on the water content of the membrane through the degree of humidification λ, that varies between 8 for low water content and 22 for high water content conditions; it is a physical parameter that represents the ratio between the moles of water contained in the membrane and the moles of silicon ions. This correlation describes properly the enhancement of performance of Nafion at high water content.
Finally, the concentration overvoltage η_{conc} is derived from Gasteiger [3] and expressed as follows:

$$\eta_{ohm} = \frac{RT}{F}\left(\frac{1}{4} + \frac{\gamma}{\alpha}\right) ln\left(1 - \frac{RT}{4F\, P_{O_2}} R_T\, i\right) \; [V] \tag{9}$$

where R_T is the oxygen transport resistance through GDL and γ is the ORR reaction order with respect to oxygen partial pressure, an empirical value found to be equal to 0.54. The total oxygen transport resistance describes the depletion of the oxygen partial pressure from the channel to the interface between catalyst layer and membrane and will have a pivotal role in the degradation analysis, whereas it increases a lot with during the lifetime [3]. The oxygen transport resistance consists of molecular diffusion resistance in GDL and permeation resistance through the ionomer film surrounding the catalyst layer agglomerates.

3.2 Degradation model

Degradation is a major challenge in fuel cell research together with limitation of catalyst loading, in order to achieve a low cost and a full deployment in the market in near future. Degradation is fundamental from an engineering point of view because it decreases voltage during the lifetime in a significative way; understanding the performance loss mechanism of voltage cycling is crucial for

the successful commercialization of the PEM fuel cell.
This aspect was long studied in literature. Bezmalinovic et al. [4] analysed cyclovoltammetry and impendance spectroscopy graphs during durability tests and managed to correlate the change in polarization curve with the increase in both activation losses and ohmic resistance. It is significant that most of degradation occurred in the first part of the test, during the first 1000 cycles and the large increase in cell resistance (almost 3 folds) can only be contributed to the increase of resistance within the catalyst layer.
In this work, the purpose is to analyse only the electrode degradation, without taking into account the membrane; then, from an analytical viewpoint, the dynamic change is assumed to affect only the activation and the concentration overvoltage. This will lead to a worsening in the reaction kinetic and increase in the oxygen transport resistance through the electrode, that are prevalent respectively at low and high current densities. On a first approximation, the Nafion membrane will be considered to preserve its original characteristics, even if many sources report about membrane thinning and increasing in ionic resistivity; that can be nevertheless a way to carry on this project.
In particular, both activation and concentration overpotential increase are analytically linked to the increase of the electrochemical surface area (ECSA), one of the electrochemical parameters used to describe the electrode activity: it's an estimation of how effective the catalyst microstructure is since it represents the total surface of the Pt nanoparticles that is useful for reactants adsorption or desorption, referred to the mass of Pt used. Indeed, it's measured in m^2/g_{Pt}. A higher ECSA means an electrode that manages to adsorbe/desorbe a larger amount of charge using the same Pt quantity.
After having performed cyclovoltammetry (CV) on different electrodes, the ECSA of Pt was determined by charge integration under the hydrogen desorption peaks appearing between 0 and 0.35 V, by assuming a charge of 210 μC/cm^2 for the electroactive Pt surface, using the following theoretical formula [4]:

$$ECSA = \frac{Q_H}{m\, q_H} \qquad [m^2 g_{Pt}^{-1}] \tag{10}$$

where Q_H (μC) is the charge of hydrogen desorption, m (μg cm^{-2}) is the Pt metal loading and q_H (μC cm^{-2}) is the charge required for desorbing a monolayer of hydrogen on a Pt surface.
During the fuel cell life, the ECSA strongly decreases: the small Pt nanoparticles of 2-4 nm diameter tend to be unstable during fuel cell operation owing to their high surface tension which leads to dissolution of platinum into the ionomer phase; this leads to a loss of ECSA via Pt particle growth and the electrochemical disconnection of several Pt particles in the ionomer phase.
The increase of both activation and concentration overvoltage are linked to the loss of ECSA through two different processes.
As explained by [3], the purely kinetic performance loss of the fuel cell due to platinum dissolution can be estimated assuming that simple Tafel kinetics apply for the oxygen reduction reaction. Then the activation overvoltage increase is calculated with:

$$\Delta\eta_{act,cath} = \frac{RT}{\alpha F} \log\left[\frac{(i_0\, ECSA)_{BOL}}{(i_0\, ECSA)_{EOL}}\right] \quad [V] \tag{11}$$

where the subscripts BOL and EOL refer to beginning-of-life and end-of-life conditions, respectively. Assuming that the exchange current density i_0 does not change significantly with the ECSA, the oxygen reduction reaction kinetic voltage loss for a 10-fold reduction in ECSA predicted would be roughly 70 mV at 80 °C. It should be noted that eq. (11) doesn't depend on the current density; this results in a translation downward of the whole polarization curve of a certain voltage gap proportional to the logarithm of the ECSA decrease. From experimental evidences, this is not enough to model the polarization change over time whereas a steep drop in the performance is evident at mid-high current density levels. For this reason, it's necessary to incorporate another contribute.

As suggested by Jomori et al.[5], the degradation has an important effect on the high current performance of the fuel cell since the oxygen transport resistance of the electrode increases during the lifetime.

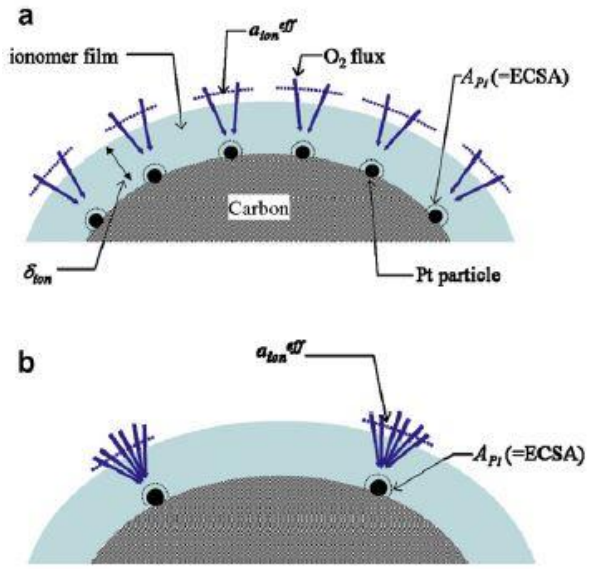

Fig. 3-2 *Schematic illustration of Pt surface area (ECSA), effective ionomer area (a_{ion}^{eff}) in catalyst layer. (a) At beginning of life. (b) After degradation.*

The oxygen transport resistance consists of molecular diffusion resistance in GDL and permeation resistance through the ionomer film surrounding the catalyst layer agglomerates:

$$R_{TOT} = R_{GDL} + R_{ion} \quad [s\,m^{-1}] \tag{12}$$

The resistance through the gas diffusion layer R_{GDL} is supposed to be constant during the lifespan since the carbon paper is very stable and doesn't experience remarkable degradation modes. On the other hand, for what concerns the ionomer resistance a more detailed representation is required, and the schematic illustration of the electrode CL is shown in fig. 3-2. Firstly, it's assumed that not all the ionomer area surrounding the catalyst site is directly used for the oxygen diffusion: only a part of the whole area is effective for the actual permeation and it's called a_{ion}^{eff}. From theoretical correlations found in [5], a_{ion}^{eff} is inversely proportional to the total oxygen transport resistance, that it's also intuitive because a lower percentage of the total ionomer area means a more difficult mass transport. Another important correlation is that, as is clear in fig. 3-2, a_{ion}^{eff} is roughly proportional to the ECSA; this assumption is experimentally validated performing measurement of transport resistance through limiting current density method for electrodes with different ECSA. Using all these assumptions leads to express the total oxygen transport resistance as a function of the ECSA, so eq. (12) transforms into:

$$R_T = \frac{C_1}{ECSA} + C_2 \quad [s\,m^{-1}] \tag{13}$$

in which C_1 and C_2 are empirical constants found to be 1700 s m^{-1} and 5 s m^{-1}, respectively. Then, from an analytical viewpoint, the decrease in ECSA during electrode lifetime causes an increase in the oxygen transport resistance; as will be clear in the following, this has a major effect at medium and medium-high current density levels.

4. RESIDENTIAL APPLICATION FEATURES

4.1 House energetic characterization

As the purpose of this work is to assess the energetic benefit that could bring the use of an innovative electrode instead of a traditional one in a µCHP system, it's necessary to have at disposal statistical data. In particular, the characteristic of a typical Canadian household were taken into account considering both the electrical power consumption and the thermal energy need.
It's well-known that the natural gas grid is capillary widespread all over Europe and North America, indeed, as presented in fig. (4-1), the most used fuel for house heating in Ontario is natural gas; this [9] is the basic requirement for a possible future installation of PEMFC devices on a large scale.

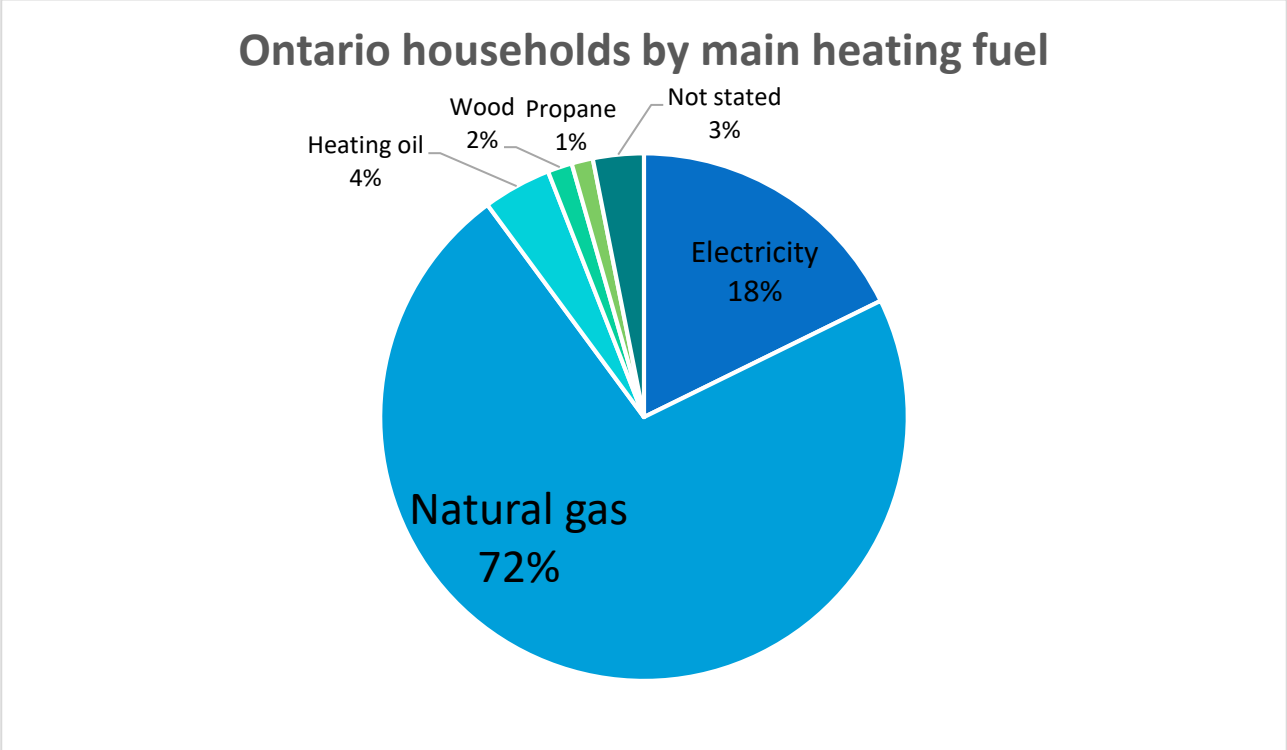

Fig. 4-1 *Energetic mix of fuel used for house heating in Ontario*

Saldanha et al. [6] compared the measured data of electrical drawn of a sample of 12 Canadian houses having different size and number of occupants. A seasonal variation in the electric profile was discovered to be very important because of the higher load that the air cooling fan must face during the summer time; besides nowadays it's common that the summertime electrical need overtakes the winter one. Table 4-1 shows the main features of the housing chosen in this work; the list of appliances is very important to understand in which time of the day will be located the power consumption peaks. The measured yearly consumption is 58,7 GJ that correspond to 16,3 MWh.

Type	Detached
Vintage	1990s
Size	195 m^2
Number of occupants	3
Main electrical appliances	Range, fridge, dishwasher, microwave, Chest freezer, clothes washer, clothes dryer, DHW heater

Table 4-1 *Characteristic of the household selected*

It should be noted that these consumption data are much higher comparing to Europe; the reasons are the colder weather and simply the more intensive energetic lifestyle [10].

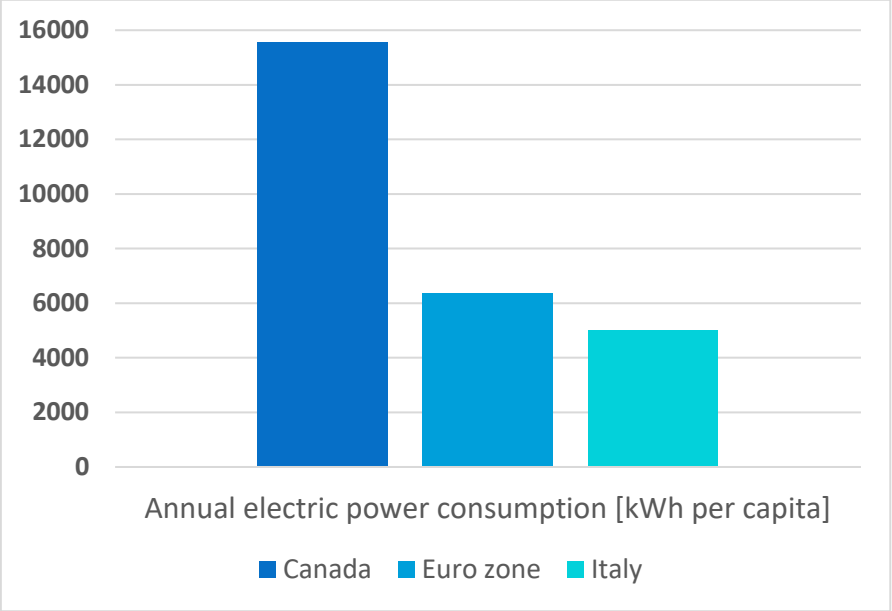

Fig. 4-2 *Comparison between average electricity consumption in different countries*

The electrical profile found is represented with a high 1-minute resolution. We can notice in fig. 4-3 two high peaks that typically happen in the morning and in the evening (more precisely 9 am and 8 pm). Moreover, as previously said, there is a significant difference between winter and summer profiles during the whole day.

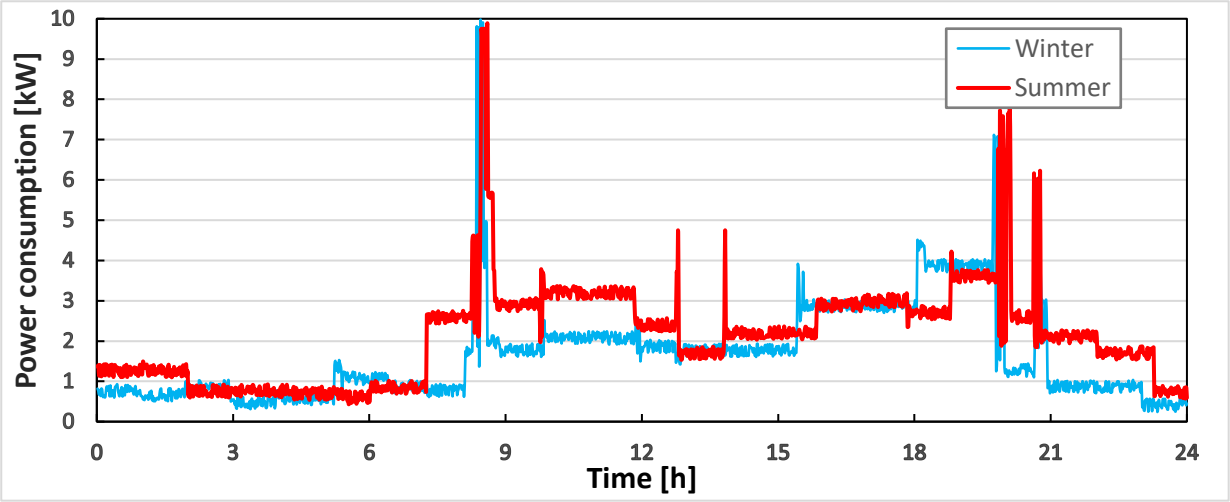

Fig. 4-3 *Electrical power daily profile*

The high time resolution is very important to locate the consumption peaks and properly model the system response in those cases. Indeed, an electrical load profile averaged on a too long timespan would result in a lack of information. Fig. 4-4 compares the measured electrical demand of the summer months with the same profile averaged on a 15 minutes interval on a restricted time interval (7 a.m. - 1 p.m.); the average configuration could be used when there aren't significant oscillations but it's clear that the peaks around 8.30 a.m. and 1 p.m. are properly highlighted only with a high-resolution approach.

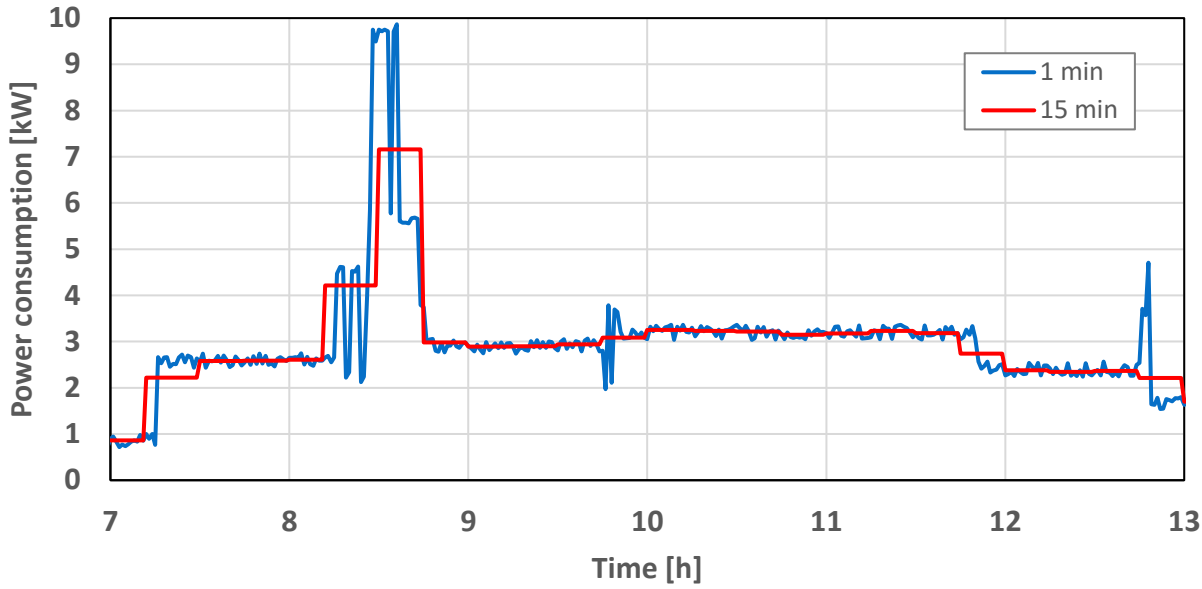

Fig. 4-4 *Comparison between different time resolutions*

On the other hand, for what concerns the thermal demand, it isn't necessary to express the energy need daily because of the characteristics of the heating system: air is used as heat-carrying fluid through a ducts system and it's assumed that the whole environment is used as a thermal energy storage to shave the demand peaks. Then, the thermal need is found to be equal to 93 GJ per house (for the Ontario province) [7]. Successively, as suggested by [8], the total year demand is split in months from September to May following a sinusoidal wave trend. Moreover, it's expected that, since the data used come from a statistical collection, the thermal need on a yearly basis will be significantly higher than the thermal energy that can be produced by a µCHP system because the currently existing housings don't have an optimal energy level; a high thermal loss is usually due to insufficient insulation. It's common believe that in innovative or upgraded households, there will be a strong development in the insulation and in the management of sun loads leading then to low energy building, so that the thermal need decreases; in that future scenario, a µCHP system based on PEMFC is expected to fully cover the thermal load. Follows that in this simulation a back-up heating system will be required to totally fulfill the thermal load.

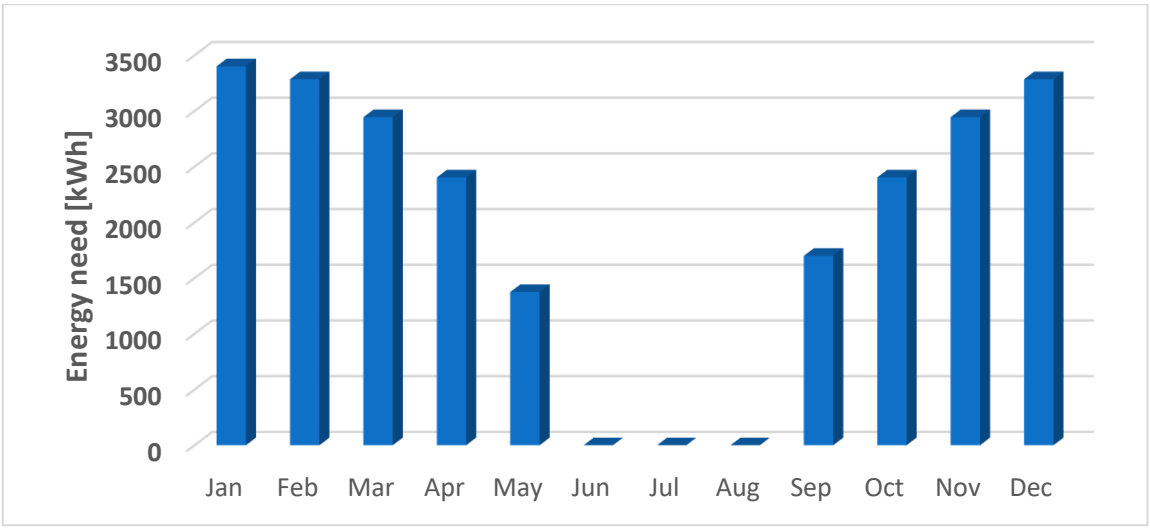

Fig. 4-5 *Thermal energy demand on a monthly basis*

4.2 Nominal point selection

The selection of nominal operating point has a direct impact on the fuel cell stack performance and efficiency. A compromise must be found between high power density and high efficiency: at low loading the efficiency is very high (around 70%) but the power produced is too low resulting in a big stack size increasing the equipment cost; on the other side, the maximum power density is assured at high current levels, where the low efficiency is not acceptable as it drops to 30%, causing a higher cost of operating cost. Then a trade off between those two extreme situations must be achieved. This is actually an intrinsic shortcoming of fuel cell technology from an engineering point of view: it is impossible to match the best efficiency with the highest power density.
The number of cells in series has been chosen following some technical specifications in literature referring to stacks of a similar power, leading to 50 cells in series for a 2 kW_{el} power stack; moreover, the nominal cell voltage is set at 0,6 V because it gives a satisfactory total voltage at the stack terminals. These two assumptions lead to the nominal values summed up in table 4-2.

Stack power	2 kW
Nominal current density	1.19 A cm^{-2}
Nominal cell voltage	0.6 V
Single cell power density	714 mW cm^{-2}
Number of series cell	50
Cell area	64.5 cm^2
Efficiency	50.4%

Table 2-2 *Nominal operation point specifications*

After choosing all the load and production system characteristics, it's easy to simulate the energetic behaviour in Matlab environment for the whole system lifetime. An algorithm compares minute-by-minute the electrical load with the polarization curve and computes electrical and thermal energy output, efficiency and fuel consumption as instantaneous quantities. Depending on the moment in the day and on the modulation configuration, the power can be the nominal one if the load is higher than 2 kW_{el}, or equal to the load otherwise (assuming that the fuell cell is instantaneously able to adjust to the load power). The following formulae are used:

$$Q_{th} = \left(-\frac{\Delta h}{2F} - V \right) I_{TOT}\, n_{cell} \ \text{[kW]} \qquad (14)$$

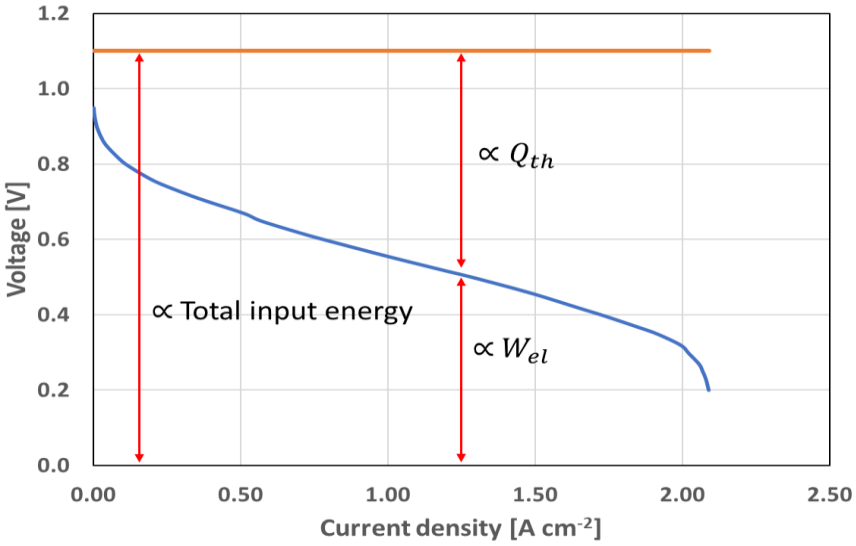

Fig. 4-6 *Energetic balance on the fuel cell*

Eq. (14) is just the analytical form of the graph in fig. 4-6. It simply follows by the application of the First Principle of Thermodynamics on the fuel cell considered as a black box, and states that the total chemical energy used as input (proportional to the variation of enthalpy linked to the hydrogen oxidation reaction Δh) is transformed for a certain amount directly into electrical power and the rest is degraded into heat. The amount of input energy transformed in power depends on the working point because at higher current densities the mass transport phenomena enhance the irreversibilities, resulting in a higher heat available.
The efficiency is expressed in a general form as the ratio between the useful output and the input required to obtain it. Therefore, for a fuel cell application the output is represented by the electrical power while the input is the energy related to the fuel used:

$$\eta = \frac{W_{el}}{G_{H_2}\, LHV} = \frac{V}{\frac{MW_{H_2}}{2\,F}\, LHV} * 100 \qquad [\%] \tag{15}$$

where G_{H_2} is the hydrogen stream (mol s^{-1}), MW_{H_2} is the molecular weight of hydrogen (g mol^{-1}) and LHV is the low heating value (J mol^{-1}). It should be noted that all the values except the voltage are constant, so the efficiency, as function of current density, can be calculated simply scaling the voltage:

$$\eta(i) = 81.37 * V(i) \qquad [\%] \tag{16}$$

A typical value of efficiency is 56.7% at 0.7 V. Finally, the fuel consumption is computed instantaneously be the algorithm using eq. (17) and at the end of the year the total fuel consumption is obtain per sum. λ is a coefficient that expresses the fuel excess not used for the reaction due to stagnation and will be assumed constant equal to 1.2.

$$G_{H_2} = \frac{I_{TOT}}{2\,F}\, MW_{H_2}\, n_{cell}\, \lambda \quad [kg\, s^{-1}] \tag{17}$$

4.3 Comparison between different operation modes

Since the load is not constant in time the fuel cell can operate with some different logics during the day. Three modulation patterns will be examined:

1. No modulation: the cell works 24 hours a day at nominal power. An exchange of power takes place in both directions between the residential user and the electrical grid: the surplus power (especially during the night) is sold to the grid and some power must be bought to face the power peaks. This is considered the basic mode because the simplest and it's expected to give the worst results in energetic terms.
2. Day-night modulation: the stack is simply turned on each morning and off each evening with an automatic control. Doing so, all the energy consumed during the night must be purchased from the grid. This configuration mode is possible for PEM devices because the low operation temperatures (between 50 and 90°C) permit a fast-starting ramp (15-30 min).
3. Load-following modulation: the stack adjusts instantaneously to the electrical demand decreasing the current density delivered at partial loading; the operating point is no longer fixed in the nominal point, but it shifts along the polarization curve. This is the most expensive solution because it requires the installation of electronic control devices. Of course, the grid connection is still necessary to face the maximum peaks.

In fig 4-7 the modulation modes are compared to the load profile (only summer, for simplicity); in all of them a certain amount of electrical power must be obtained by the grid because of the high peaks in the morning and evening. The configuration without modulation is expected to be the worst from an economical point of view: prices at which energy locally produced is sold to the grid are usually very low so it's better to avoid producing energetic surplus. On the other side, this configuration is the simplest from a technical viewpoint because it doesn't require any electronic device control. For these same reasons, the load-following modulation is the most promising solution because it minimizes the energy sold to the grid and especially shows an efficiency significantly enhanced when working at partial load (during night); this results in a saving in the yearly fuel consumption. Eventually, it's difficult to allege a priori if using a day-night modulation would be interesting permitting to reach better performances: that depends on the average power consumed during the night.

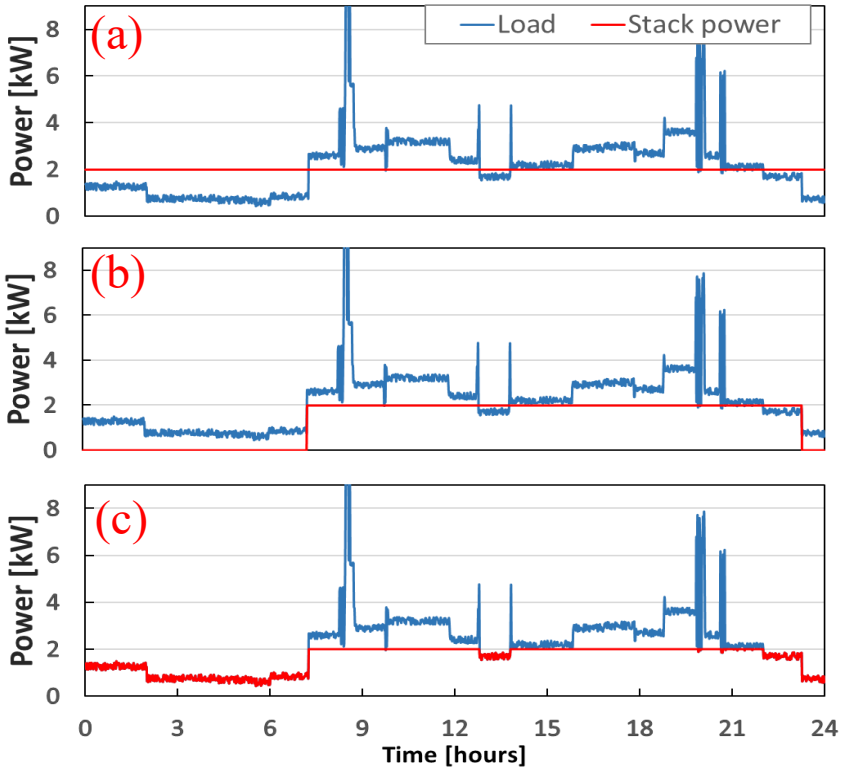

Fig. 4-7 *Comparison between different modulation configuration: (a) no modulation, (b) day-night modulation and (c) load-following*

5. RESULTS

5.1 Performance results

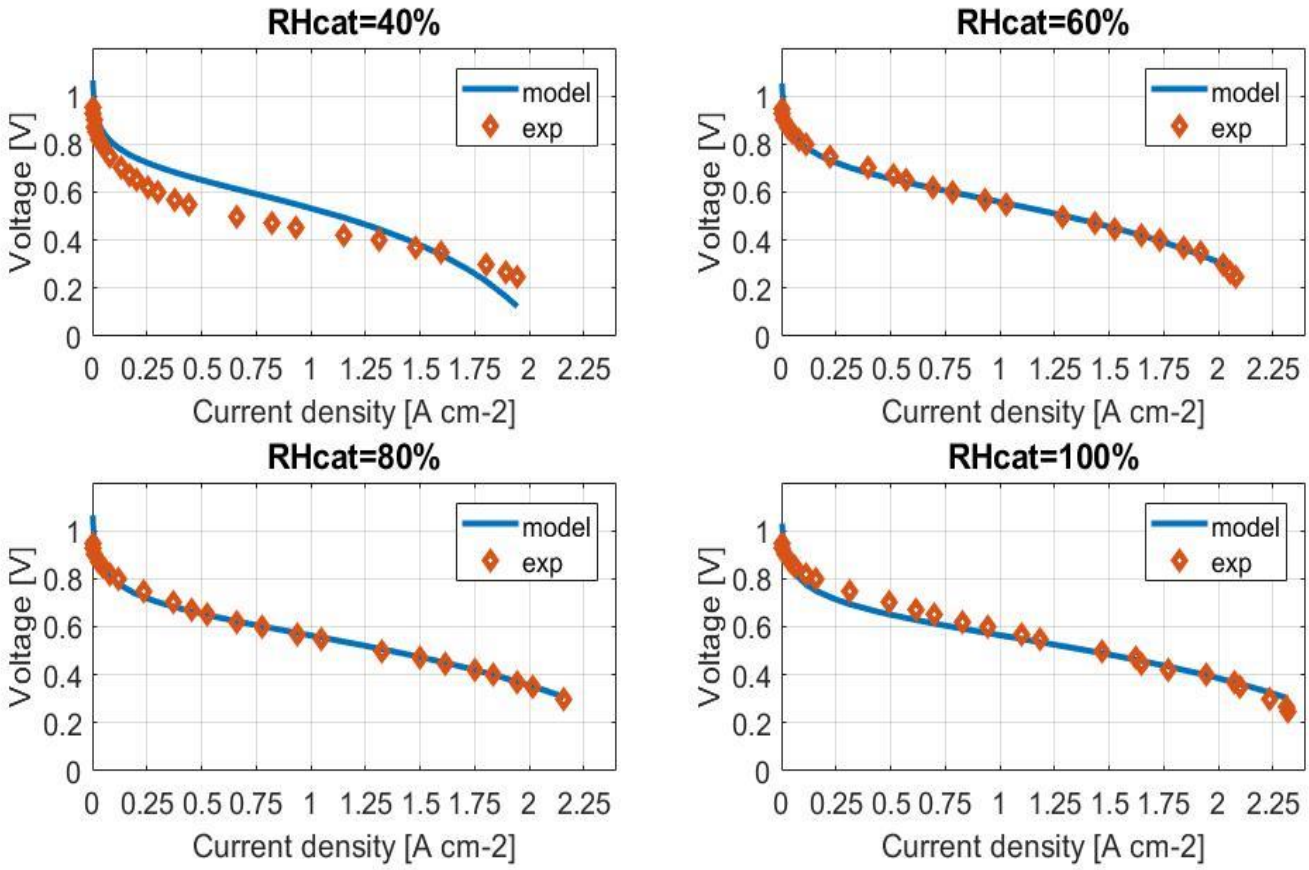

Fig. 5-1 *Model expectation and actual measurement comparison of Nafion based electrode*

Description of MEA	Hot-press conditions	Operating conditions
▪ 20% Pt/C Premetek ▪ 0.18 mg/cm^2 Pt loading ▪ GDL - SGL 29 BC ▪ Nafion NRE 212	▪ Temperature – 100°C ▪ Pressure – 40 kg/cm^2 ▪ Time – 3 minutes	▪ H2/pure O2 gas feeds ▪ Cell temperature 80°C ▪ Back pressure 10 psi ▪ Anodic RH 100% ▪ Cathodic RH varying from 40% to 100%

Table 5-1 *MEA characteristics and testing conditions*

The SGL 29 BC was chosen as GDL because of its good performance in removing water. The fuel cell tests were performed using pure H_2 and O_2 as reactant flows. Gases passed through a humidifier bottle before entering the cell and the bottle temperature was varied to adjust the relative humidity of both anodic and cathodic streams. In fig. 5-1 the upshot of the comparison between the experimental results and the model expectation is shown. The polarization curves were measured at a fixed temperature (80 °C) and anodic relative humidity (100%) while the cathodic relative humidity varies from 40% to 100%, in order to test the model reliability. Tab. 3-1 sums up the characteristic of the electrode and also the test conditions. The result seems to represent quite well the voltage response at all the operational conditions except the lowest humidity of 40%. The curves show the same trend at low current densities and the important pattern is that the model describes

well the performance dependence on the cathodic relative humidity: in fact, the change in slope of the polarization curve is consequence of the different humidification level of the membrane, that decreases the protonic resistance associated with the membrane.
For what concerns the tests with SS-CCE, the MEA specifications were kept the same (tab. 3-1) and as expected the performance are quite the same with respect to the Nafion based electrode. As already discussed, the advantage of SS-CCE lays in the dynamic performance during the lifetime because it shows a lower degradation. Unfortunately, the comparison is made only at one level of relative humidity (40%) because of lack of data.

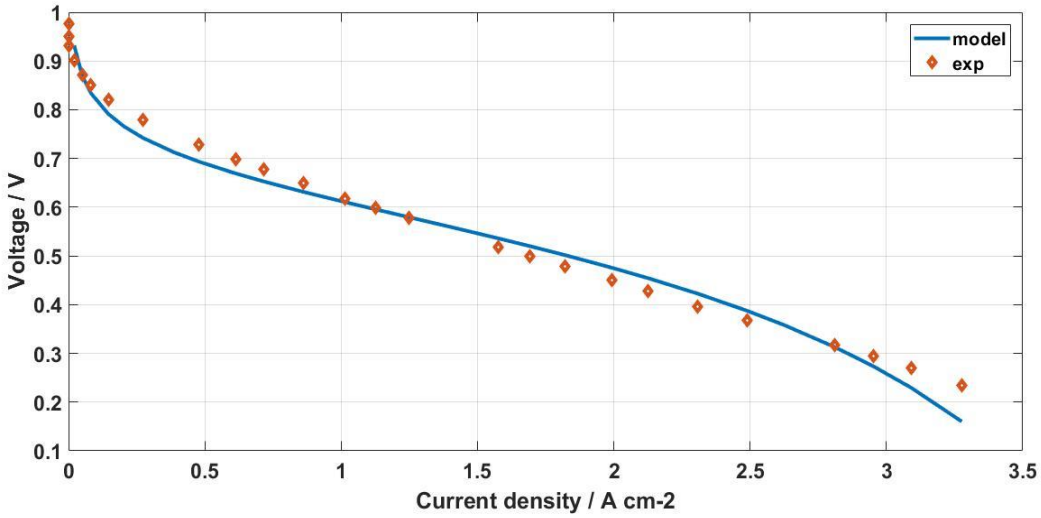

Fig. 5-2 *Model expectation and actual measurement comparison of Nafion based electrode of SS-CCE*

Also in this case, the model shows a good description of the data found in laboratory (fig. 5-2); this result is not surprising because from a performance point of view the SS-CCE and Nafion based electrodes are very similar [1].
In conclusion, as a result of the satisfying approximation found using the GSSEM with both Nafion-based and SS-CCE electrodes in the single cell configuration, it will be used in the following treatise to forecast the performance of the whole fuel cell stack in a real residential application, paying particular attention to the degradation feature.

5.2 Static residential performance

Tab 5-2 shows the comparison in energy consumption for a PEM fuel cell stack using Nafion based electrodes with different operation modes. The self-consumed energy is instantaneously transferred from the stack to the load; the energy received from the grid is necessary to fulfill the peaks (especially in the morning and afternoon); finally, for certain operating conditions it's possible to exchange energy with the grid during night hours (i.e. when load power is lower than the stack rated power). It should be noted that the total annual energy requirement is exactly equal to the sum of energy self-consumed and energy bought from the grid.

	Self consumption energy		Energy received from the grid		Surplus energy sold	Average efficiency	Fuel consumption
	kWh/y		kWh/y		kWh/y	-	m^3/y
No modulation	12.745	77%*	3.701	23%*	4.535	50.4%	11.717
Night-day	10.410	62%	6.037	38%	-	50.4%	7.059
Load-following	12.745	77%	3.701	23%	-	57.3%	8.642

Table 5-2 *Final energetic outcome. Comparison among different operation configurations*

The configuration mode without any modulation and with a night-day modulation are similar from an energetic point of view; operating without a modulation creates a large energy surplus during the night hours and could be interesting if there were high incentives from the government for the power produced and sold to the national grid. They have the same average efficiency (50.4%) because both work at the nominal power point. Switching the stack off during night means buying the night electric demand from the grid and it's not a negligible amount of energy, in fact the share of energy covered with respect to the total decreases from 77% for the "no modulation" case to 62% for the night-day mode. Of course, the fuel consumption is reduced of the same ratio. As expected, the load-following mode is the most promising configuration. The energy covered is exactly the same of the no-modulation mode because the stack power and the profile are the same; the big improvement is in the fuel consumption (that decreases of almost one third) because during night the stack works with a much higher efficiency because of the partial load, this leading also to a higher average efficiency (57%).

5.3 Degradation results

Before showing the degradation model outcome, it's important to describe in detail the laboratory procedure for the measurement of ECSA. Electrode durability was examined by exposing each MEA (both Nafion based and SS-CCE) to an accelerated stress test (AST). During the AST, the cathode was exposed to nitrogen and the anode was exposed to hydrogen with flow rates of 200 and 100 ml min^{-1} respectively. The cell temperature was held constant at 25 °C, as was the anode and cathode humidifiers held constant at 25 °C. The AST consisted of 4000 potential cycles between 0.05 and 1.35 V vs reference hydrogen electrode (RHE), with periodic assessment of electrode health by cyclic voltammetry (CV) that gives also a measurement of the electrochemically active surface area. All electrochemical measurements were performed by using a Solartron 1470E Multichannel potentiostat and paired with Solartron 1260 frequency response analyzer, controlled using Multistat software (Scribner Associates). Measurements were performed in triplicate for each MEA composition.

In fig 5-3 the CVs during the AST are shown for both Nafion based and SS-CCE electrodes (data are available from a previous work [1]). The CVs exhibit three characteristic regions: the hydrogen adsorption and desorption region at low potential range, the double layer capacitance region between 0.35 and 0.50 V and the Pt oxide formation and reduction region at high potentials. As already mentioned, the ECSA is proportional to the area below the hydrogen adsorption/desorption peaks appearing between 0 and 0.35 V (at the left), so we can observe a huge decrease in the Nafion based electrode, much higher than the SS-CCE. For the Nafion based electrode, only the first and last CVs are reported for lack of data.

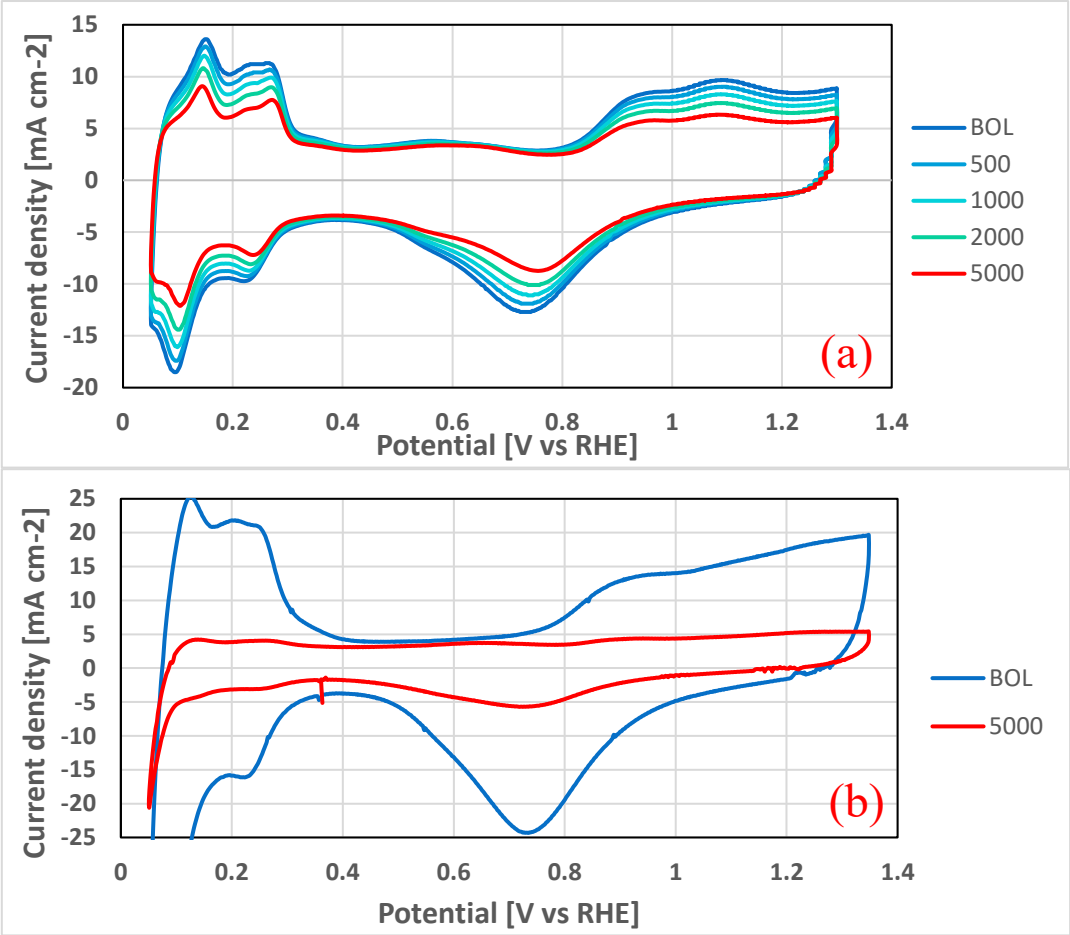

Fig. 5-3 *(a) SS-CCE and (b) Nafion based electrode CVs durind the durability tests*

The final comparison of ECSA vs lifetime is given in fig. 5-4. The data collected match the results reported in literature [3] where, after a rough decrease in the first part of the test (up to the 2000th cycle), the ECSA stabilizes asymptotically to a certain value. The advantage of the SS-CCE with respect to the Nafion based electrode is clear: after the whole test the SS-CCE shows a decay around 26% while the Pt-C electrode loses over 90% of its initial chemical activity. That will result in a significant difference in the drop of performance between fuel cell stacks using different electrodes. Choosing the same working time, the SS-CCE experiences a lower decrease in the polarization curve.

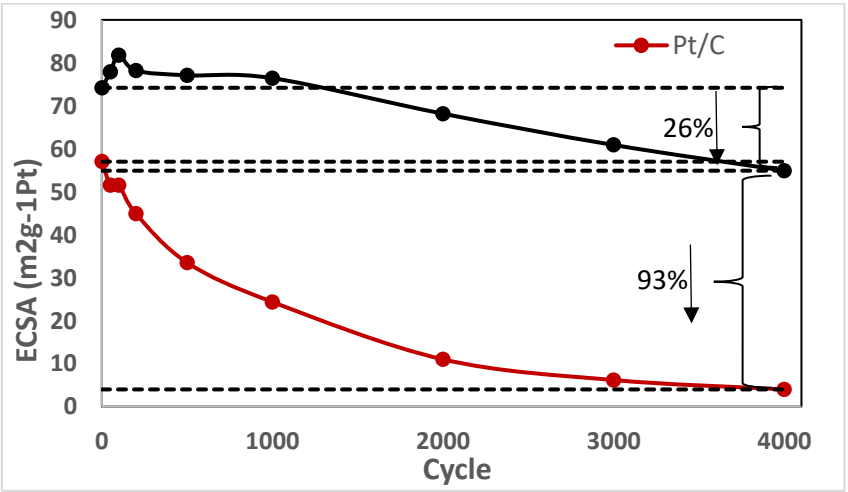

Fig. 5-4 *ECSA decrease during AST for Nafion-based and CCE*

Fig. 5-5 shows the performances at the beginning and at the end of the life (BOL and EOL respectively), for a Nafion based support electrode (MEA properties are listed in tab. 5-3); also model outcomes for both configurations are reported. Error bars are used for the end of life model output since the measurement of the ECSA through CV is intrinsically affected by an error.
The model describes with a good approximation the polarization curve at the beginning of life; this result is actually similar to the result obtained in the static model section, since the electrodes used have a similar Pt loading (0.18 and 0.2 mg cm^{-2}) even if the Pt-C used were produced by different companies. Passing from BOL to EOL, the trend is very different especially at high current density levels: in the region above 0.7-0.8 A cm^{-2} the huge increase in oxygen transport resistance makes infeasible a practical use of the MEA after a high number of cycles. The model represents also the EOL performance quite well; a good result is represented by the fact that the model output polarization curve drops very fast to low voltages (circa 0.3 V) at mid current density levels (between 1 and 1.5 Acm^{-2}). Nevertheless, the model has two significant lacks that are stressed in the comparison between the expectation and the laboratory outcome.
First of all at very low current density, where the activation overvoltage is predominant, the model is too optimistic in the performance resulting in a voltage too high; that is true up until 0.25 A/cm^{-2} circa so it doesn't affect in a big way the power output.
Secondly, there is a non-negligible difference between the model output and the experimental results, equal to 0.1 V for a wide interval of current densities. This can be explained by an empirical evidence: as reported in [1], the post-mortem analysis after the AST revealed a huge Pt migration from the CL to the interface between membrane and electrode. The Pt nanoparticles that migrated are still useful and active for the electrochemical reaction, but aren't any more detectable by a CV for the ECSA estimation; this leads to a underestimation of the performance due to a huge decrease in the number of active Pt nanoparticles, that actually in part just migrated.

Description of MEA	Operating conditions
▪ 20% Pt/C Johnson Mattey ▪ 0.2 mg/cm^2 Pt loading ▪ GDL - SGL 29 BC ▪ Nafion NRE 212	▪ H2/pure O2 gas feeds ▪ Cell temperature 80°C ▪ Back pressure 14 psi ▪ Anodic RH 100% ▪ Cathodic RH 100%

Table 5-3 *MEA specifics and testing conditions*

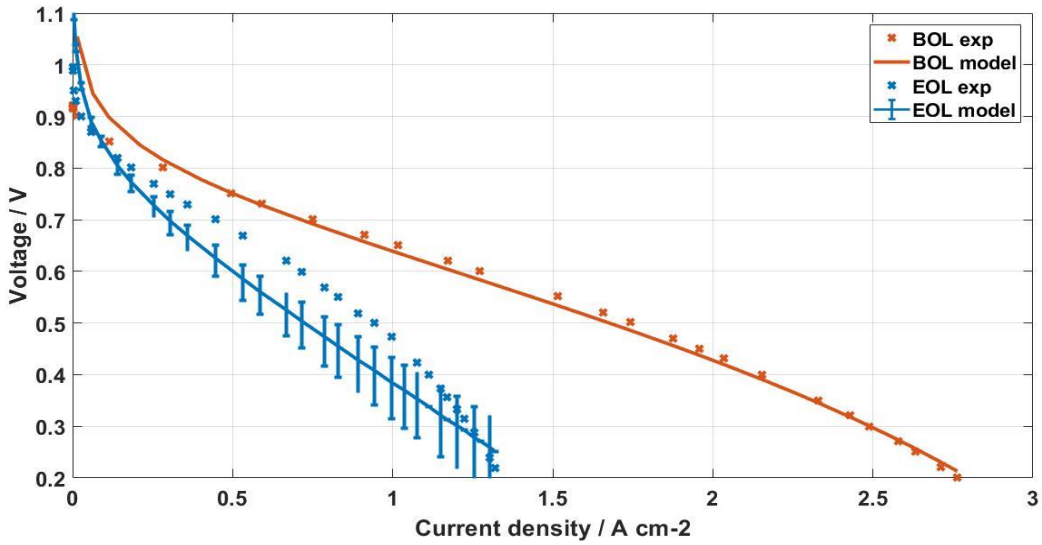

Fig. 5-5 *Test results and model output at beginning of life (BOL) and end of life (EOL) for Nafion based electrode*

Cycle	ECSA [m^2/g_{Pt}]		Error [m^2/g_{Pt}]
	SS-CCE	NAFION	
1	80.6	72.7	-
500	74.0	42.5	± 3
1000	63.9	35.4	± 3
2000	57.0	25.3	± 3
3000	49.5	20.7	± 3
5000	43.6	15.3	± 3

Table 5-4 *ECSA decrease over AST cycles for both electrodes under study*

Fig. 5-6 reports the model output of the same electrode at different cycles during the AST. Unfortunately, the polarization curves weren't tested at intermediate cycles because of the risk of breaking the membrane, so it's impossible to make a comparison between the model and the real response. Still, it's interesting to note that the polarization curve decrease is strongly non-linear with respect to the ECSA reduction (tab. 5-4); that shouldn't be a surprize since there are many sources of non-linearity in the physics behind the phenomenon.

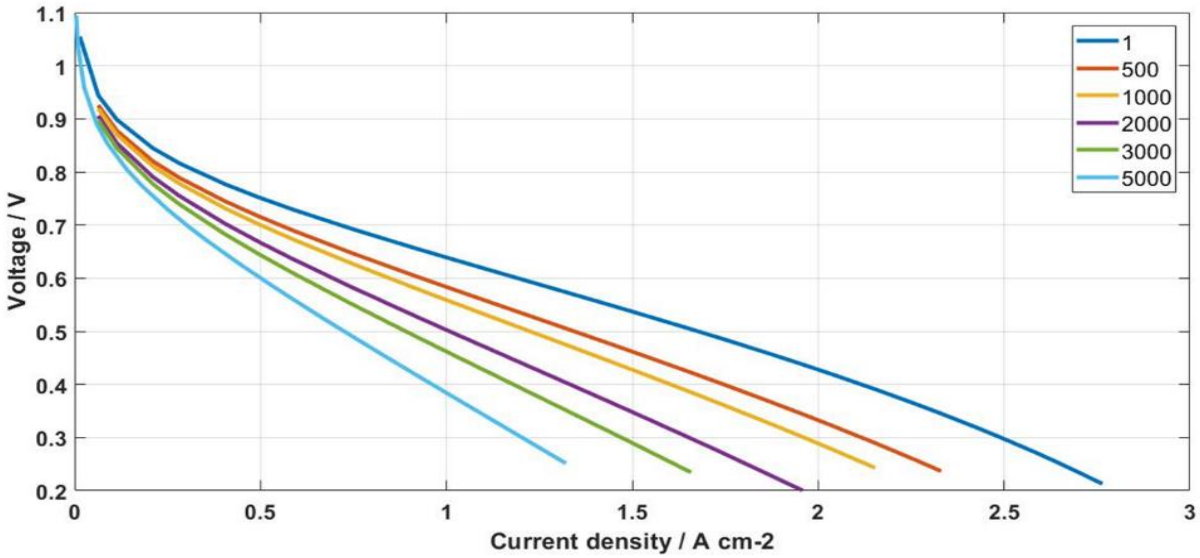

Fig. 5-6 *Degradation model output at different cycles*

A durability test was performed for the SS-CCE electrode following the same procedures. The MEA characteristics were kept the same in order to isolate the dependence on other patterns like Pt loading and membrane thickness (tab. 5-3). The test conditions were equal as well.
In fig. 5-7 the comparison between the model output and the actual laboratory response is shown and in tab. 5-4 the decrease in ECSA is reported as function of cycles. First of all, the error bars are less important with respect to the previous case because the model is less sensitive at high ECSA values.
As for the Nafion based electrode, the model is not very reliable at low current density levels (below 0.25 A cm^{-2}), whereas there is an important overestimation. Nevertheless, the behaviour of the electrode after the AST is well modelled for medium and high current density levels.

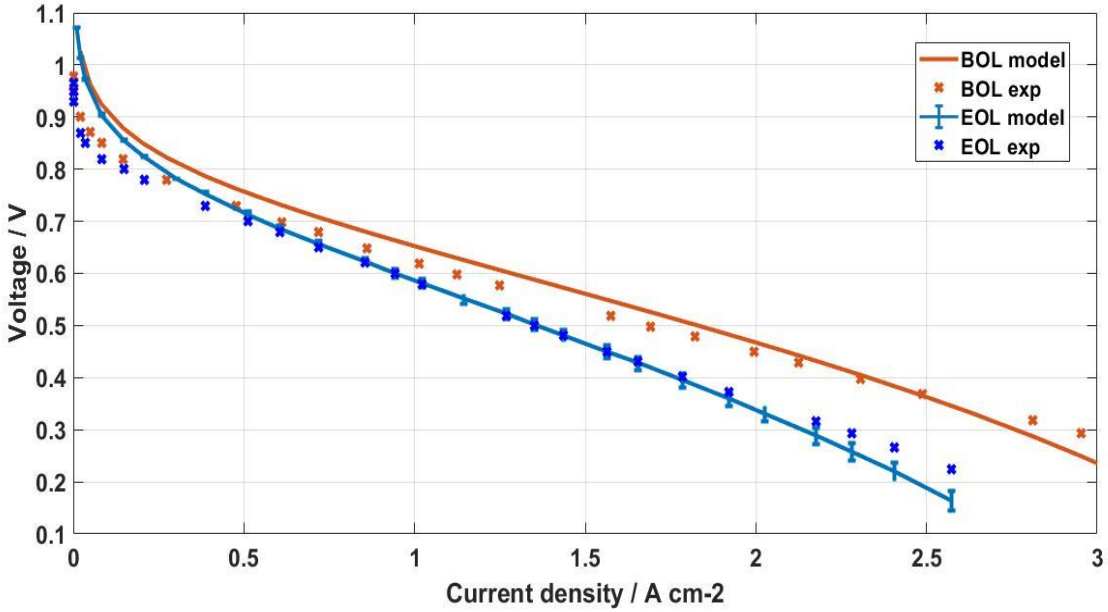

Fig. 5-7 *Test results and model output at beginning of life (BOL) and end of life (EOL) for SS-CCE*

A worthy feature of this degradation model is that it doesn't depend directly on a time reference, such as hours of working or electrode age; it receives as input the ECSA that in turn depends on the operating time. This is very convenient because it's suitable to describe the fuel cell dynamic behaviour for any type of final use destination, even if they may be intrinsically characterized by degradation rate very different. For example, a fuel cell stack used for an automotive application experiences several start-up and shut-down cycles in short time, and also during the working period the load varies depending on the output power required; on the other hand, a stationary application works for most of life at nominal point with few or almost null shut-down periods, so it's subjected to a degradation much lower. Tab. 5-5 shows the durability 2020 targets by application (found in [11]); the threshold taken into consideration is 15% in voltage decrease and the difference in lifetime among distinct application could be of one order of magnitude. One may argue that the limit of 15% voltage loss is too strict since after that decrease the fuel cell performance is still satisfactory from a technical point of view; nevertheless, that limit is chosen because of economic constrains.

Application	**Durability (hours @ <15% voltage loss)**
Transportation	5,000
Consumer Electronics (<50W)	5,000
Auxiliary Power Unit (3–30kW)	35,000
Stationary	40,000

Table 5-5 *Typical lifespan values for different purpose technologies*

5.4 Domestic application

Moving now to the residential application discussion, the same threshold used in tab. 5-5 was considered; in this sense, the expected result is that the SS-CCE electrode will take a longer time to reach such a voltage decrease with respect to the Nafion-based electrode because of the smoother ECSA degradation trend.

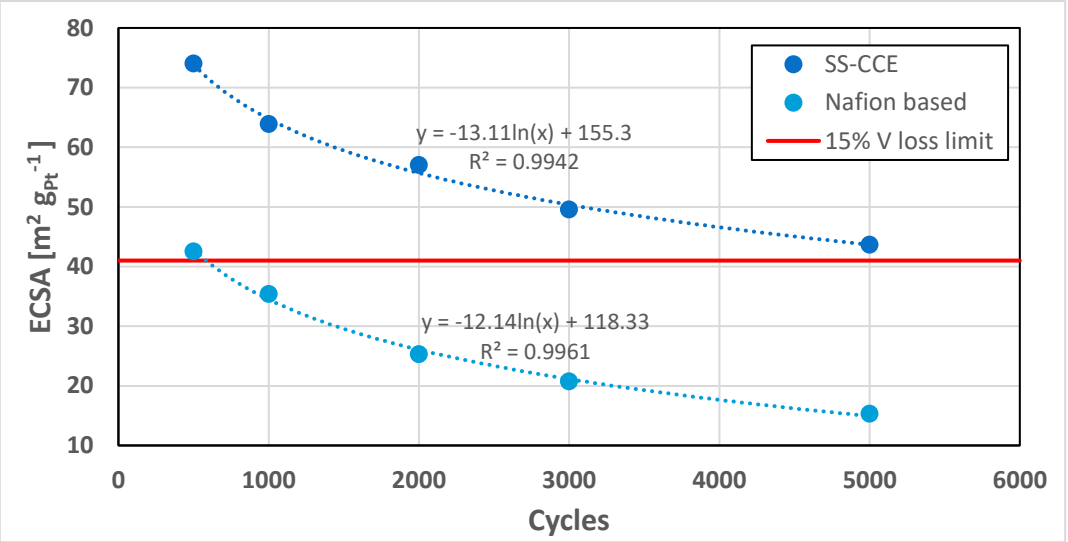

Fig. 5-8 *ECSA decrease trendlines and voltage loss limit in red*

First of all the ECSA decrease over time was found to be well approximated with a logarithmic law for both electrodes, as suggested by [3], and fig. 5-8 shows the trendlines.
Afterwards, the purpose was to find the ECSA value corresponding to a 15% voltage reduction, and that's possible running the model with different values obtainable from interpolation; the result is 41.7 m^2 g_{Pt}^{-1} (fig. 5-8) and this is the limit corresponding to the chosen voltage loss, common to both the electrode types. The efficiency, being directly proportional to the voltage, of course will decrease of the same percentage as the voltage. The electrodes under study will reach the ECSA limit value in different times that can be estimated by their trends; this leads to a maximum number of cycles of 550 for Nafion electrode and over 5000 for the SS-CCE.
Since the polarization curve, an own parameter of the cell, changes in time, the nominal point will have to adjust to this change. Assuming that the power delivered at the stack terminal remains the same (equal to the rated one), the cell power density is constant during the lifetime and a voltage decrease requires then an increase in the current density (from 1.19 A cm^{-2} to 1.5 A cm^{-2}). In fig 5-9 the nominal point shift is highlighted.

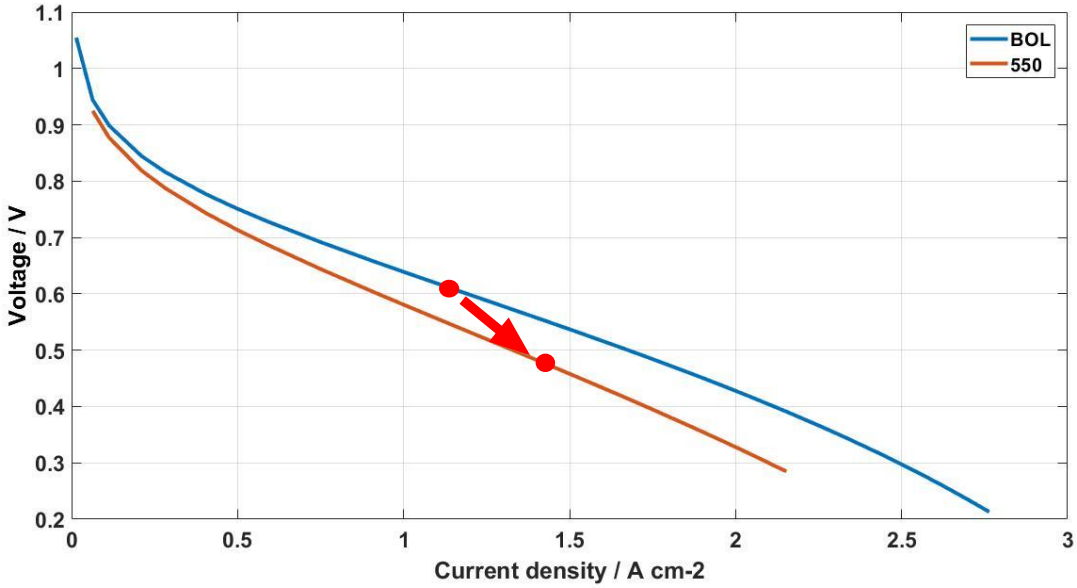

Fig. 5-9 *Nominal point shift due to degradation*

Passing from the laboratory stress test to the real working conditions is not straightforward: many circumstances might have a huge impact on the durability, such as the limited control of gas flow and humidity level, frequent temperature variation and the instability of reactants quality. The AST is done in extremely harsh conditions since the electrode experiences sudden and continuous voltage cycles from low to high voltage values. Then it's important to correlate one single cycle of the AST to a suitable time unit that can be used in the operation of a real stack. In the case of load-following configuration, we can distinguish two different conditions: during the day the cell works at the nominal power or close, while during the night it works at partial loading. Then we can assume that the electrodes experience a daily voltage change between the nominal value (0.6 V) and a value corresponding to low current density (so above 0.9 V). From this proceeds the assumption that one single AST cycle corresponds to one day since the voltage excursion is similar. Following this line of reasoning, considering the Nafion based electrode, a voltage reduction of 15% corresponds to 550 cycles, so 550 days (equal to 13,200 hours) for the real stack. That value has the same order of magnitude of typical lifespans that can be found in literature for the same kind of application and size (tab. 5-4). Analogously, for the SS-CCE, this method would lead to an estimated lifetime of 4500 days that is 108,000 hours; this value of life is not realistic for current PEMFC technology but we must consider than it is estimated taking into account only the ECSA loss as voltage decrease cause, while there could be other failure modes on such a long span, linked to the membrane (thinning or even breaking) or to carbon corrosion.

	Power stack [kW]	Claimed life duration
Ballard	4 - 21	>20,000 h
	0.4 - 3.3	10,000 h

Table 5-4 *Declared lifetime of fuel cell stack*

5.5 Comparison in µCHP system performance

The comparison in the µCHP system performance will be made with the same stack nominal power (2 kW_{el}); whereas the purpose is to assess the difference in energy consumption during the whole lifetime, the dimensional parameters such as number of cell n and cell area A will be kept the same for both electrodes (see tab. 2-2), so that the amount of space occupied is the same.
Through the system simulation it's possible to calculate, for the whole lifetime (550 days for the Nafion-based electrode and 4500 for the SS-CCE), the monthly fuel consumption and the average efficiency at which the fuel cell stack operates, taking into account the working hours at partial loading. Values of electrical power (self-consumed and purchased from the grid) were already discussed in section 5.2 for the BOL configuration and in the time-depending study they don't change.
As previously found, the life for the SS-CCE electrode is almost 10 times longer than the traditional one and this represents the main strong point. Nevertheless, we can compare the performance based on the same time interval, equal to the lifetime of the Nafion based electrode (fig. 5-10). First of all, we can notice the strong difference in the energy use between summer and winter, due to the change in load profile. Secondly, the Nafion based electrode hydrogen consumption has an increasing trend due entirely to degradation that makes the consumption at the end of life circa 15% higher than how it was at the beginning; on the other hand, it's clear that the SS-CCE fuel consumption is constant over the time considered.

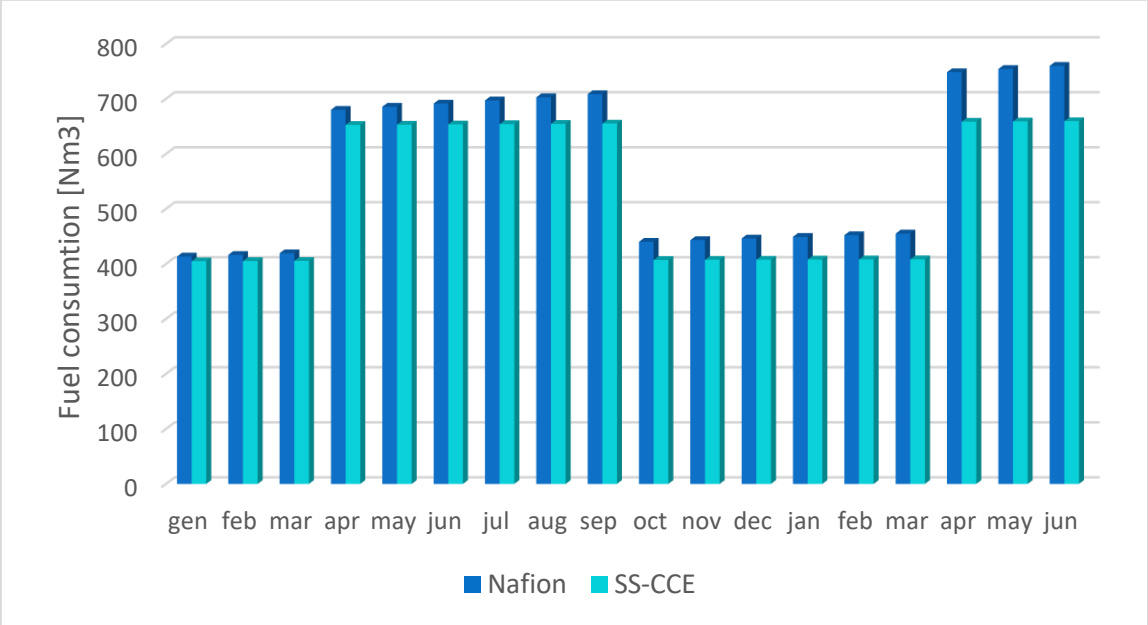

Fig. 5-10 *Fuel consumption during lifetime*

As a result of the degradation, also an efficiency worsening can be measured: this is much more evident for the Nafion based electrode. In tab. 5-5 I reported efficiency values related to various steps: nominal efficiencies at beginning of life (BOL) and at the 550th cycle (that represents the end of life only for the Nafion based electrode) can be calculated with eq. (16); the average efficiencies are instead computed minute-by-minute through the Matlab simulation.
At the beginning of life, the both the nominal and average efficiencies are comparable even if the Nafion based electrode has a slightly better performance. At the end of life, the latter shows a decrease in the nominal efficiency of 15%, equal to the voltage loss chosen as reference; at the contrary the SS-CCE has a negligible loss of just 1%. Comparing the average efficiency with the nominal, for both electrodes the average is higher because of the working periods at partial loading during night. Lastly, taking into account the contrast between the average efficiency at the BOL and at the 550th day, the Nafion based electrode shows a significant drop (from 57.5% to 48.5%); on the other hand, the SS-CCE electrode has a quite null worsening (from 57.5% to 57%) and it's a remarkable result that it reaches almost 60%.

		Nafion	SS-CCE
BOL	η_{nom}	48.8%	47.2%
	$\eta_{average}$	57.5%	57.5%
550th day	η_{nom}	39.0%	46.3%
	$\eta_{average}$	48.5%	57.0%

Table 5-5 *Efficiency drop during lifetime*

6. CONCLUSION

A model was found in literature for the prediction of performance of fuel cell in static conditions and it was validated with actual experimental data. Since degradation is a very important issue for fuel cell technology, it was token into consideration through some patterns in order to expresses the time-depending voltage worsening; the final result is a model able to predict the performance at the beginning of life as well as at any cycle during the lifespan, using the electrochemical parameter ECSA as a detector of degradation. Then, a certain value of voltage reduction is used as threshold beyond which it's no more profitable to use the fuel cell. Through the model, it's possible to link this value of voltage decrease to a certain value of ECSA loss, so that reaching it means arrive at the end of life for any fuel cell technology.
Lastly, a comparison in both static and dynamic conditions between two different electrocatalyst is performed: a novel SS-CCE and a traditional Nafion based electrode. As expected, the novel electrode is much more stable towards degradation because its microstructure manages to stabilize better the Pt nanoparticles, resulting in a lower ECSA loss during time; this advantage is quantitatively estimated simulating the behaviour of a μCHP system facing both electrical and thermal loads of a typical Canadian household over the whole lifetime.

7. REFERENCES

[1] R. Alipour Moghadam Esfahani, H. M. Fruehwald, F. Afsahi, and E. B. Easton, "Enhancing fuel cell catalyst layer stability using a dual-function sulfonated silica-based ionomer," *Appl. Catal. B Environ.*, vol. 232, no. March, pp. 314–321, 2018.

[2] M. W. Fowler, R. F. Mann, J. C. Amphlett, B. A. Peppley, and P. R. Roberge, "Incorporation of voltage degradation into a generalised steady state electrochemical model for a PEM fuel cell," *J. Power Sources*, vol. 106, no. 1–2, pp. 274–283, 2002.

[3] P. Zihrul, I. Hartung, S. Kirsch, G. Huebner, F. Hasché, and H. A. Gasteiger, "Voltage Cycling Induced Losses in Electrochemically Active Surface Area and in H $_2$ /Air-Performance of PEM Fuel Cells," *J. Electrochem. Soc.*, vol. 163, no. 6, pp. F492–F498, 2016.

[4] Á. Kriston, T. Xie, D. Gamliel, P. Ganesan, and B. N. Popov, "Effect of ultra-low Pt loading on mass activity of polymer electrolyte membrane fuel cells," *J. Power Sources*, vol. 243, pp. 958–963, 2013.

[5] S. Jomori, N. Nonoyama, and T. Yoshida, "Analysis and modeling of PEMFC degradation: Effect on oxygen transport," *J. Power Sources*, vol. 215, pp. 18–27, 2012.

[6] N. Saldanha and I. Beausoleil-Morrison, "Measured end-use electric load profiles for 12 Canadian houses at high temporal resolution," *Energy Build.*, vol. 49, pp. 519–530, 2012.

[7] "Households and the Environment : Energy Use," no. 11, 2011.

[8] RDHBuilding Engineering Ltd, "Energy Consumption and Conservation in Mid and High Rise Residential Buildings in British Columbia," vol. 1, p. 264, 2012.

[9] http://oee.nrcan.gc.ca/corporate/statistics/

[10] https://data.worldbank.org/indicator/EG.USE.ELEC.KH.PC?end=2014&locations=CA-IT-XC&start=2014&view=bar

[11] US department of energy

8. ACKOWLEGMENTS

I would like to thank my advisors, Stefania Specchia and Bradley Easton, and all the research group that helped me in this project during my mobility program, especially Reza Alipour and Richard Acheampong. I'm very thankful to them all.